Neutron and *β/γ* Radiolysis of Water up to Supercritical Conditions. 1. *β/γ* Yields for H₂, H• Atom, and Hydrated Electron

Dorota Janik, Ireneusz Janik, and David M. Bartels*

Radiation Laboratory, University of Notre Dame, Notre Dame, Indiana 46556

Received: March 3, 2007; In Final Form: June 7, 2007

Yields for H_2, H• atom, and hydrated electron production in *β/γ* radiolysis of water have been measured from room temperature up to 400 °C on a 250 bar isobar, and also as a function of pressure (density) at 380 and 400 °C. Radiolysis was carried out using a beam of 2−3 MeV electrons from a van de Graaff accelerator, and detection was by mass spectrometer analysis of gases sparged from the irradiated water. N_2O was used as a specific scavenger for hydrated electrons giving N_2 as product. Ethanol-d_6 was used to scavenge H• atoms, giving HD as a stable product. It is found that the hydrated electron yield decreases and the H• atom yield increases dramatically at lower densities in supercritical water, and the overall escape yield increases. The yield of molecular H_2 increases with temperature and does not tend toward zero at low density, indicating that it is formed promptly rather than in spur recombination. A minimum in both the radical and H_2 yields is observed around 0.4 kg/dm³ density in supercritical water.

I. Introduction

Commercial nuclear reactors essentially provide a source of heat used to drive a "heat engine" (turbine) to create electricity. A fundamental result of Thermodynamics shows that the higher the temperature at which any heat engine is operated, the greater its efficiency. Consequently, one obvious way to increase the operating efficiency and profitability for future nuclear power plants is to heat the water of the primary cooling loop to higher temperatures. Current pressurized water reactors run at roughly 300 °C and 100 atm pressure.[1] Designs under consideration would operate at 500 °C and 250 atm,[2−6] i.e., well beyond the critical point of water. This would improve the thermodynamic efficiency by about 30% and allow considerable reduction in cost. A major unanswered question has been, what changes occur in the radiation-induced chemistry in water as the temperature and pressure are raised beyond the critical point, and what do these imply for the limiting corrosion processes in the materials of the primary cooling loop?

Direct measurement of the chemistry in reactor cores is extremely difficult. The extreme conditions of high temperature, pressure, and radiation fields are not compatible with normal chemical instrumentation. There are also problems of access to fuel channels in the reactor core. For these reasons, all reaction vendors and many operators have extensively used theoretical calculations and chemical models to simulate the detailed radiation chemistry of the water in the core and the consequences for materials.[7,8] The results of these model calculations can be no more accurate than the fundamental information fed into them, and serious discrepancies remain between model calculations and reactor experiments.[8,9] The problem of modeling a supercritical-water-cooled reactor is even more daunting. A number of studies have been published in the last several years with the aim of providing the necessary fundamental information needed to model radiation chemistry in supercritical water.[10−23] Both reaction rates and radiation yields (*G*-values) for the primary free radicals •OH, H•, and e_{aq}^- are required, as well as for the recombination products H_2 and H_2O_2. Moreover, in reactor cores radiation is deposited both via *γ* radiation and energetic neutrons;[24] this paper represents the first in a series that will report *G* values from both *β/γ* radiation and neutrons using the same detection methodology.

To transfer the information to other systems for modeling studies, it is very important to know precisely the temperature and pressure of the fluid under irradiation. This is much easier to achieve with a flowing system than with sealed samples. For neutron experiments a high-temperature flow system was constructed for a small nuclear reactor at the University of Wisconsin, as will be described in subsequent papers. As a source of low-LET radiation for high-temperature experiments, we have found it very convenient to use an electron beam from a 3 MeV van de Graaff accelerator. The choice of detection method and scavengers is dictated by the characteristics of the reactor. The simplest method with sufficiently high sensitivity, reliability, and versatility is the detection of stable gas products produced by the radiation[25] using a mass spectrometer.

In the following section we describe in some detail the detection technique that is common to both experiments. The scavenging experiments and results are then described, and in the Discussion we compare these results with others in the literature.

II. Experimental Section

The *β*-radiolysis experiments were performed at the Notre Dame Radiation Laboratory using a custom-made supercritical water (SCW) irradiation block and 2.5 MeV electrons from a 3.0 MeV van de Graaff (VdG) accelerator. The apparatus consisted of sample reservoirs and pumps, a high pressure/temperature irradiation flowtube, and ambient pressure/temperature analysis setup with a directly coupled mass spectrometer (Figure 1).

Two glass water reservoirs with copper or stainless steel connection lines under atmospheric pressure were used to supply

* To whom correspondence should be addressed. E-mail: bartels@hertz.rad.nd.edu. Phone (574) 631-5561. Fax: (574) 631-8068.
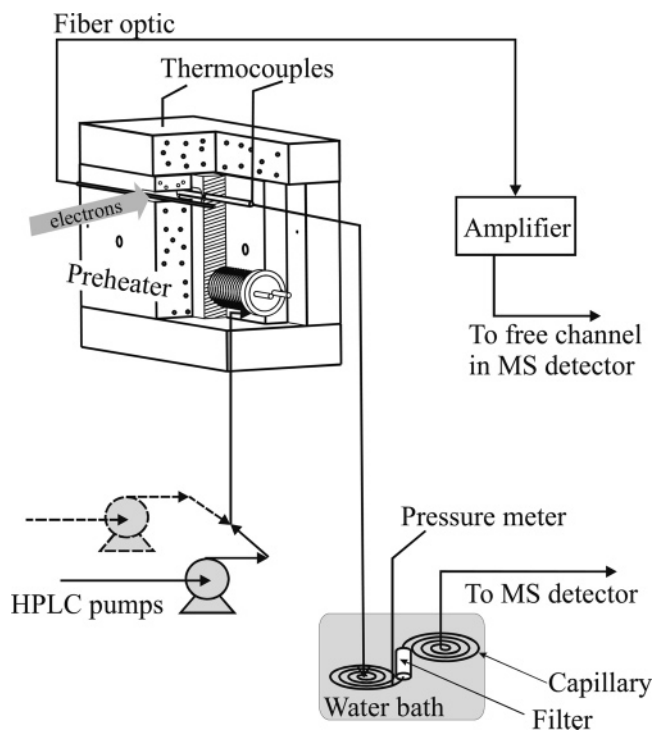
Figure 1. Experimental setup for the detection of gaseous products formed during radiolysis of aqueous solutions at high temperature and pressure.

two independent Alltech 301 HPLC pumps. The final composition of the solution was achieved by changing the flow ratio of the two pumps, keeping the total flow at 6 mL/min. All experiments used water purified by the Serv-A-Pure Co. cartridge system (resistivity 18 MΩ cm, total organic carbon <5 ppb as CO_2) and the solutions were bubbled with the required gases. A mixture of 20% H_2 in N_2 was used for mass spectrometer (MS) calibration, a mixture of 10% N_2O in Ar was used for the yield measurements, and ultrapure Ar was the sparging gas in the MS detection system. All gases were UHP from Mittler Supply, Inc. Absolute ethyl alcohol (200 proof, Aaper Alcohol and Chemical Company), deuterated ethanol CD_3CD_2OD (Cambridge Isotope Laboratories, Inc., anhydrous, 99+ atom % D), and phenol (Aldrich, redistilled, 99+ %) were used as received from vendors.

The high temperature/pressure flow cell consisted of two partially separated sections. In the lower section the solutions were pumped through Hastelloy $1/16$ in. tubing that was wrapped around a cylindrical electric heater (1000 W, 120 V). Then, after preheating, solution was introduced to an irradiation zone made from $1/8$ in. titanium tubing (0.06 mL total volume) in the upper section. Behind the irradiation zone a second cartridge heater (250 W, 120 V) was placed to maintain the temperature and compensate for the electron beam heating. The temperature of solution before and after the irradiation zone was monitored with a pair of type-K thermocouples with readout by Omega CN77000 temperature controllers whose accuracy is specified as ±0.4 °C. The entire assembly was enclosed in a stainless steel block (with a window cut for easier electron penetration through the irradiation volume) and placed in an insulating box (Rescor Ceramic Board, Cotronics Corp.). A fiber-optic was placed in a slit in the insulation in front of the irradiated tubing to monitor the dose by means of generated Cerenkov light and fluorescence. The optical signal was detected by a silicon photodiode and was monitored in one of the spare A/D channels in the MS (Pfeiffer Vacuum Prisma) along with the molecular ion signals.
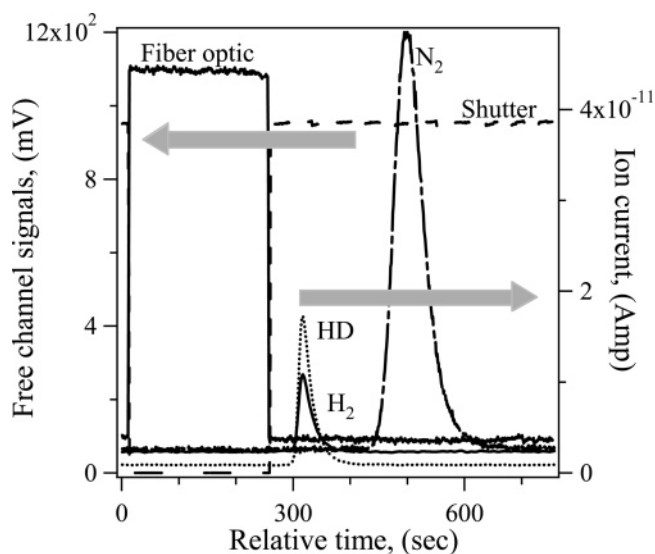

Figure 2. Set of typical molecular ion current signals (right side axis) and associated shutter current and fiber optic (free channel) signals (left axis) for 0.02 *m* EtOH-d_6 and ~2.5 × 10^{-3} *m* nitrous oxide saturated aqueous solution (at 300 °C and 250 bar).

To maintain stable temperature and pressure conditions during measurements, the flow rate through the system was kept constant. To provide a stable pressure drop, a 0.004 in. i.d. $1/16$ in. capillary was immersed in a temperature-controlled water bath. Before reaching the capillary, solution was cooled in the heat exchanger, consisting of several coils of $1/16$ in. Hastelloy tubing immersed in the same water bath, and passed through a 5 μm filter. Changing the temperature of the water bath changes the viscosity of the solution to provide precise back-pressure control at a given flow rate. Pressure in the system, with an overall stability of roughly ±0.5 bar during each single run, was monitored with a calibrated pressure transducer (OMEGA PX01 series) and strain gage meter (OMEGA DP25B-S). The manufacturer's specification is for ±0.2 bar accuracy of the pressure measurement. After reaching the lower temperature/ pressure in the water bath, the solution flows through 15 m of $1/16$ in. stainless steel tubing (i.d. 0.01 in.) to the detection setup outside the radiation vault.

To analyze dissolved gases, precisely 12.0 mL (2 min collecting time at flow 6 mL/min) of irradiated solution was collected in the sparging vessel, and then bubbled with UHP argon. The argon stripped out any gaseous products from the irradiated solutions and carried them through the water trap (0.25 in. o.d., 3 m long coiled column packed with 4A Molecular Sieves) toward the inlet of the MS capillary. The capillary, made from 3 cm long and 25 μm i.d. fused silica uncoated tubing (Chrompack), was placed in the side arm of a T-connection to allow sampling from the center of the main gas stream. The dimensions of the capillary provided optimal 10^{-5} mbar vacuum pressure in the MS chamber. The sampling stream was introduced directly into the closed HS W ion source. Molecular ion signals of the gaseous products were monitored as a function of time with a Balzers/Pfeiffer QMS 200 quadrupole mass spectrometer.

Radiolysis experiments were performed using a dc electron beam to produce absorbed doses in the range 100−700 Gy. The maximum dose was limited by the concentration of solvated electrons generated during the experiment. Final concentrations larger than 2.5 × 10^{-4} *m* would imply over 10% conversion of the available N_2O. This concentration corresponds roughly to 1000 Gy and was never exceeded during the course of the
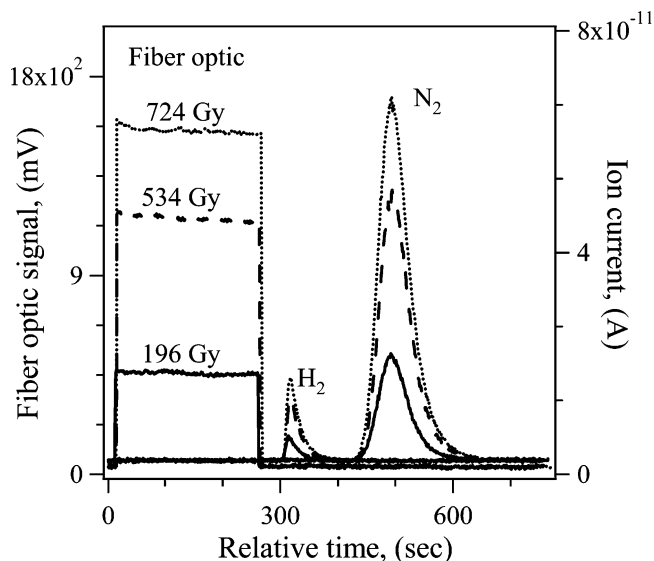
Figure 3. Typical set of collected traces for one set of conditions (0.01 *m* PhOH at 300 °C and 250 bar), for three different dose rates. Signal axes as in Figure 2.
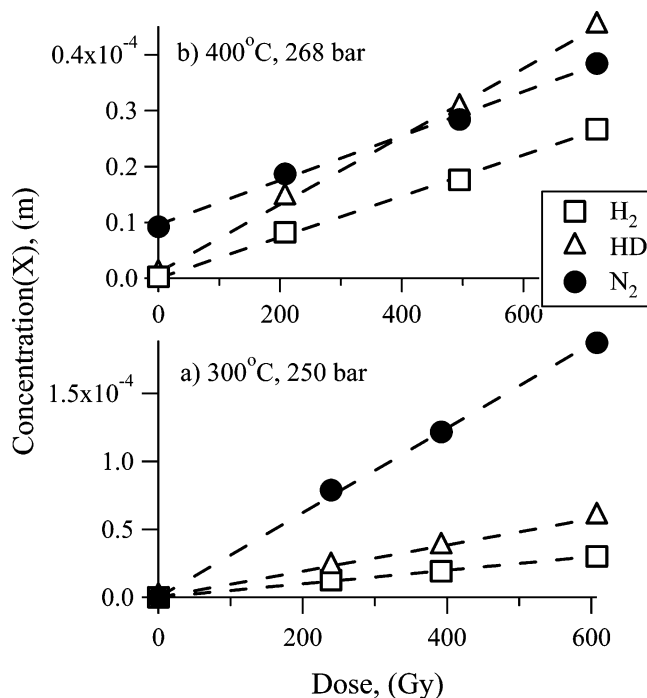

Figure 4. Linear mass spectrometer signals vs dose (a) with zero intercept and (b) a signal at 400 °C with nonzero intercept due to the thermal breakdown of N_2O.

experiments. Solutions were in the irradiation zone for 0.6 s, which for the applied doses corresponds to a dose rate of 300−1200 Gy/s.

A typical set of signals registered during a single experimental run is presented in Figure 2. The left axis corresponds to the signals registered in the detector channels monitoring the dose: the solid line represents signal from the fiber optic and the dashed line represents current on the electron beam shutter. The right axis corresponds to the molecular ion currents for the gases monitored during measurement. At the start of a run the shutter current signal is high and the fiber optic signal is low. After 15 s of baseline collection the shutter was opened and irradiation started. At this point the shutter signal disappears and simultaneously the fiber optic signal appears (see Figure 2). Irradiation was continued for the next 4 min and 30 s. Two minutes after the beginning of irradiation the process of collecting sample in the sparging vessel started. After 2 min the vessel containing 12 mL of irradiated solution (6 mL/min flow rate) was switched from the supplying line to sparging argon gas with a three way valve. After starting the sparging process the shutter was closed, as reflected in the change of corresponding signals in Figure 2. The sparged out gaseous products were carried to the MS through the water trap, which acts like a GC column to separate the products in time. H_2 and HD reached the ionizing chamber in the MS approximately 30 s after the sparging start time. Nitrogen appeared 2 min later.

The procedure presented above was typically repeated for three different doses at a given temperature and pressure (see the example in Figure 3). A relative "dose area" was obtained by integrating the fiber optic signal from 105 s up to 225 s, which corresponds to the 2 min of sample collection. Absorbed dose, D_{abs} (Gy), was calculated using

$$D_{abs} = [N_2] \times G(N_2)^{-1} \times d^{-1} \qquad (1)$$

where $[N_2]$ is measured nitrogen concentration (mol/dm^3), $G(N_2)$ is the known radiation yield of N_2 from solvated electron scavenging at room temperature (mol/J), and d is the density of water (kg/dm^3). This measurement was carried out every day to calibrate the fiber optic as a relative dosimeter for the given beam focusing conditions. A precise estimation of the radiation chemical yields of the measured products with the applied

scavenger concentrations was carried out with the stochastic simulation package described by Pimblott and co-workers.[26−29] For 0.01 *m* ethanol solution saturated with 2.5×10^{-3} *m* N_2O (which was routinely used for calibrating the fiber optic response) values of 2.84×10^{-7} and 7.91×10^{-8} mol/J were calculated at 25 °C for N_2 and H_2, respectively. The ratio $G(N_2)/G(H_2)$ obtained at room temperature agreed very well with the simulated values.

In the dose range used, the signals were a linear function of the applied dose. In most cases, the intercept of a plot of yield vs applied dose went through zero (Figure 4a). However, for conditions where thermal background decomposition was possible or suspected, a blank was measured in the absence of radiation (Figure 4b) and was included in the fit. At temperatures of 380 °C and above, nitrogen was observed as a result of decomposition of nitrous oxide on the tubing walls. The measured amount varied depending on the history of the cell walls and if it became too high, the tubing walls could be passivated by flowing O_2 gas overnight at 450 °C. At 400 °C slight decomposition of ethanol-d_6 took place (1−2 μM of HD observed). Because radiation yields were calculated on the basis of the slopes of the dose dependence, we assume that the background thermal chemistry does not affect the yield values.

The data in Figure 4 illustrate the very high precision we are able to attain in these measurements. With three or four points in each linear fit, we obtain standard deviations of the slope below 3% (typically 1%) in all of the constant pressure measurements up to 350 °C. At supercritical temperatures the scatter is slightly larger, with 7% standard deviation as a worst case, probably due to a slight drift in density during an experiment which would change the absorbed dose. The numbers are also sensitive to the calibration of the MS sensitivity carried out for each day. These calibration measurements also have standard deviations on the order of 1%. All of the measurements are made relative to the yield of N_2 in N_2O/ethanol solution at 25 °C, as explained above. Given the high precision, one can hope for accuracy on the order of 5% up to

TABLE 1: Temperature Dependence of Radiation Yields of Gaseous Products in Phenol and Ethanol Aqueous Solutions in the Presence of N$_2$O (2.5 × 10^{-3} *m*) Measured at a Constant Pressure of 250 bar

| | | $10^{-7}G(X)$ (mol/J) | | | | |
| | | in 0.01 *m* PhOH | | in 0.02 *m* EtOH-d_6 | | |
temp (°C)	density (kg/dm^3)	H$_2$	N$_2$	H$_2$	HD	N$_2$
22	1.0000	0.45	3.02	0.44	0.18	2.83
100	0.9696	0.48	3.37	0.47	0.51	3.23
200	0.8813	0.54	3.62	0.51	0.78	3.55
225	0.8527	0.55	3.69			
250	0.8209	0.57	3.74	0.56	0.95	3.65
275	0.7848	0.63	3.75			
300	0.7430	0.67	3.64	0.67	1.30	4.19
325	0.6926	0.71	3.57			
350	0.6271	0.75	3.40	0.82	1.98	4.02
380	0.4508	0.45	1.35	0.86	2.48	1.23
400	0.1665	1.09	2.03	1.72	2.92	1.93

TABLE 2: Density Dependence of Radiation Yields of Gaseous Products in Phenol and Ethanol Aqueous Solutions in the Presence of N$_2$O (2.5 × 10^{-3} *m*) Measured at a Constant Temperature of 380 °C

| | $10^{-7}G(X)$ (mol/J) in 0.01 *m* PhOH | | | $10^{-7}G(X)$ (mol/J) in 0.02 *m* EtOH-d_6 | | |
density (kg/dm^3)	H$_2$	N$_2$	density (kg/dm^3)	H$_2$	HD	N$_2$
0.1229	0.75	2.31	0.1218	2.16	5.26	3.74
0.1542	0.74	2.08	0.1617	1.67	4.54	2.59
0.2045	0.65	1.73	0.1980	1.39	4.01	1.76
0.2501	0.51	1.43	0.2567	1.24	3.36	1.52
0.3116	0.44	1.12	0.2934	1.07	2.83	1.42
0.3599	0.32	1.16	0.3639	0.89	2.57	0.94
0.4004	0.34	1.05	0.4018	0.77	2.43	1.25
0.4524	0.38	1.20	0.4540	1.03	2.92	2.05
0.4547	0.45	1.25	0.5126	1.06	3.04	4.07
0.5010	0.73	2.27	0.5430	1.10	2.83	4.68
0.5501	0.81	3.12				

TABLE 3: Density Dependence of Radiation Yields of Gaseous Products in Phenol and Ethanol Aqueous Solutions in the Presence of N$_2$O (2.5 × 10^{-3} *m*) Measured at a Constant Temperature of 400 °C

| | $10^{-7}G(X)$ (mol/J) in 0.01 *m* PhOH | | | $10^{-7}G(X)$ (mol/J) in 0.02 *m* EtOH-d_6 | | |
density (kg/dm^3)	H$_2$	N$_2$	density (kg/dm^3)	H$_2$	HD	N$_2$
0.1223	1.05	1.84	0.1211	2.06	3.14	2.24
0.1485	0.96	1.77	0.1518	1.86	3.15	1.95
0.2124	0.74	1.53	0.2124	1.73	2.81	1.81
0.2594	0.62	1.43	0.2594	1.54	2.49	1.67
0.3090	0.65	1.38	0.3090	1.32	2.29	1.61
0.3574	0.59	1.35	0.3574	1.32	2.22	1.60
0.4174	0.57	1.48	0.4094	1.33	2.35	1.51

350 °C, and perhaps 10% in the supercritical regime. Particularly in the latter regime, one also assumes accuracy of the temperature and pressure measurements to calculate the density to correct for absorbed dose. All of the experimental conditions reported below in Tables 1−3 were repeated at least once on different days. We report results from a final set of experiments in which the measurement technique had reached its ultimate precision.

III. Results

During water radiolysis a number of transient and stable products are produced. The initial reaction can be summarized with

$$H_2O \xrightarrow{\text{irr}} e_{aq}^-, \ ^\bullet OH, \ H^\bullet, \ H^+, \ OH^-, \ H_2O_2, \ H_2 \qquad (2)$$
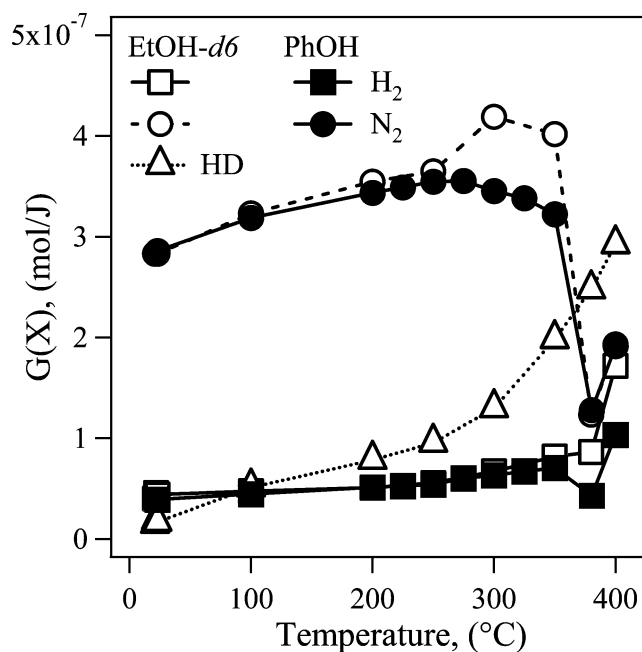
Figure 5. Radiation yields of gaseous products during radiolysis of 0.02 *m* EtOH-d_6/2.5 × 10^{-3} *m* N$_2$O aqueous solution compared with products from 0.01 *m* phenol/2.5 × 10^{-3} *m* N$_2$O solution as a function of temperature at a constant pressure of 250 bar.

It should be understood that the "yields" of H$^+$, e$_{aq}^-$, $^\bullet$OH, and H$^\bullet$ in particular are functions of time because of fast recombination. Scavenged yields of these species, typically for the first-order scavenging rate or "scavenging power "(i.e., rate constant times scavenger concentration) of 1.0×10^7 s^{-1}, are very well established at room temperature.[30] N$_2$O is well-known as a useful and very efficient hydrated electron scavenger.[31] Its reduction in reaction 3 leads to the stable gas nitrogen.

$$e_{aq}^- + N_2O \xrightarrow{H_2O} \ ^\bullet OH + OH^- + N_2 \qquad (3)$$
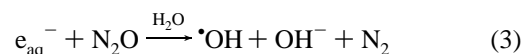
This reaction has an activation energy of 15.5 kJ/mol up to 300 °C. Above 300 °C the rate shows non-Arrhenius behavior and rate constants up to 400 °C are at least several times higher than at room temperature.[13] N$_2$O appears to be reasonably stable in supercritical water. All these facts suggest that irradiating aqueous nitrous oxide solutions should allow us to determine escape yields of e$_{aq}^-$ by monitoring production of N$_2$ over a wide range of temperatures. However, N$_2$O can also react with H$^\bullet$ atoms giving the same product in reaction 4.[32]

$$H^\bullet + N_2O \rightarrow \ ^\bullet OH + N_2 \qquad (4)$$
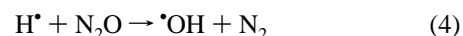
The relatively small rate coefficient (2.5 × 10^6 M^{-1} s^{-1}) for this reaction at room temperature does not guarantee the same at higher temperatures. From pulse radiolysis studies we found that at 350 °C, the reaction 4 rate constant is approximately 1.5×10^8 M^{-1} s^{-1}.[33] However, the detailed temperature dependence in the entire range up to 400 °C is still unknown.

Among many possible scavengers phenol molecules are known to react rapidly with both $^\bullet$OH and H$^\bullet$ atoms but quite moderately with electrons.[16,31] The reaction with e$_{aq}^-$ reaches a maximum rate of 6.5 × 10^7 M^{-1} s^{-1} at ca. 125 °C, and by 200 °C becomes slower than at room temperature, so it should not be any issue at still higher temperatures.[34] Phenol is well-known to be quite stable in supercritical water. Addition of

Neutron and β/γ Radiolysis of Water

J. Phys. Chem. A, Vol. 111, No. 32, 2007 **7781**
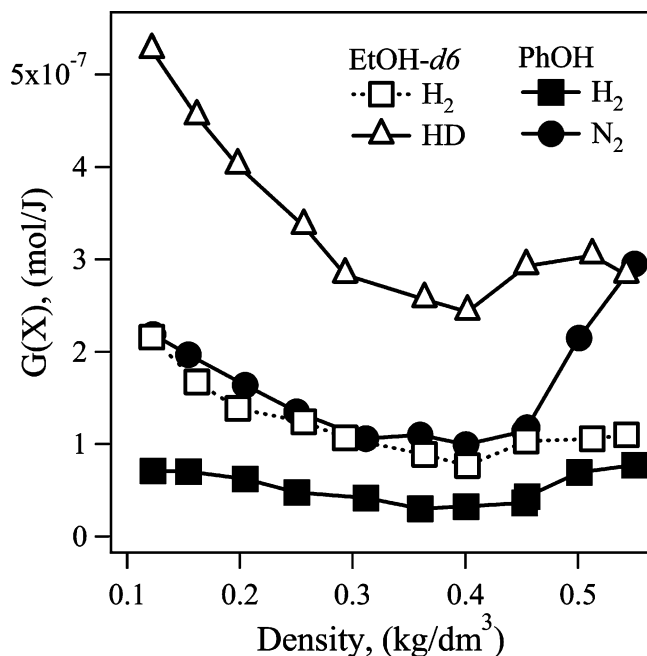
Figure 6. Comparison of radiation yields in deuterated ethanol and phenol solutions vs density at 380 °C.
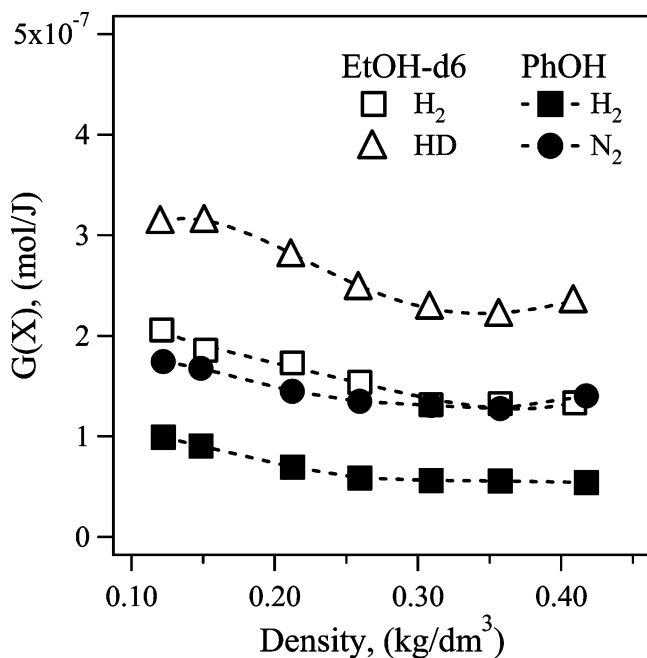
Figure 7. Comparison of radiation yields in deuterated ethanol and phenol solutions vs density at 400 °C.

0.01 *m* phenol to 2.5×10^{-3} *m* N$_2$O/water initiates scavenging of •OH radicals and formation of dihydroxycyclohexadienyl radicals via reaction 5[35,36] ($k_5 = 6.6 \times 10^9$ M^{-1} s^{-1}). A similar addition reaction (6) is observed for H• atoms leading to hydroxycyclohexadienyl radical[31] ($k_6 = 1.7 \times 10^9$ M^{-1} s^{-1}).

$$\bullet OH + PhOH \rightarrow \text{dihydroxycyclohexadienyl radical} \quad (5)$$

$$H\bullet + PhOH \rightarrow \text{hydroxycyclohexadienyl radical} \quad (6)$$

The temperature dependence of these rate constants has been measured recently in our laboratory up to 400 °C.[16] Reaction 6 occurs much faster than reaction 4, so the N$_2$ and H$_2$ radiolysis

yields in the N$_2$O/phenol system should correspond to the solvated electron and molecular hydrogen formed in spurs, respectively.

Radiation yields of gases produced during β-radiolysis of 0.01 *m* phenol aqueous solutions in the temperature range 22–400 °C for isobaric conditions (250 bar) are presented in Figure 5. Detailed values are listed in Table 1. From room temperature up to 275 °C a steady increase in yield was observed for both N$_2$ and H$_2$. At 275 °C nitrogen yield reached a maximum of 3.55×10^{-7} mol/J, then started decreasing to a minimum of 1.28×10^{-7} mol/J at 380 °C. The hydrogen yield kept increasing up to 350 °C but then dropped to a minimum of 4.30×10^{-8} mol/J at 380 °C. For both hydrogen and nitrogen the sudden yield drop occurs around the water critical temperature of 374 °C, and yields increase again after the temperature increases to 400 °C.

It has been shown that the density of water has a major impact on the yields of transient species in water under supercritical conditions.[10,17] In this range we have chosen two temperatures to illustrate the effect of density, 380 and 400 °C. The flow was kept constant and the density in the sample was adjusted by changing the pressure in the system. The molal (*m*) concentration of solutes was the same as in the isobaric experiments described above. In the range 0.12–0.55 kg/dm^3 at 380 °C, the density dependence of radiation yields in Figure 6 displays a U-like shape for both N$_2$ and H$_2$, with minima near 0.40 kg/dm.^{3} In a narrower range of 0.12–0.42 kg/dm^3 at 400 °C, we observed similar behavior of both yields, but with a less pronounced decrease at intermediate density as illustrated in Figure 7. Our pumps did not allow us to extend the measurements to higher densities (pressures) at this temperature. Detailed values for density dependence at 380 and 400 °C are listed in Tables 2 and 3, respectively.

The experiments performed with the phenol/N$_2$O solution give us solid information about molecular hydrogen as well as solvated electron radiation yields over a wide range of temperatures and densities. In fact, these experiments were performed because of problems found with the preferred scavenging system of N$_2$O with ethanol-d_6, as will now be described. Both hydrogen atoms and hydroxyl radicals abstract hydrogen from ethanol carbons, forming α- and β-hydroxyethyl radicals (C$_2$H$_4$OH)•, as shown in reactions 7 and 8 with overall room-temperature rate constants as indicated.

$$H\bullet + C_2H_5OH \rightarrow H_2 + (C_2H_4OH)\bullet$$
$$k_7 = 2.0 \times 10^7 \text{ (M}^{-1}\text{ s}^{-1})^{[31]} \quad (7)$$
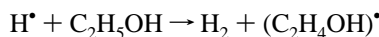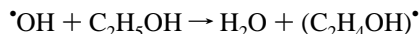
$$\bullet OH + C_2H_5OH \rightarrow H_2O + (C_2H_4OH)\bullet$$
$$k_8 = 1.9 \times 10^9 \text{ (M}^{-1}\text{ s}^{-1})^{[31,37,38]} \quad (8)$$

The hydrogen abstraction from the alcoholic hydroxyl group in reaction 9 is of minor importance (2.5%)[39] at room temperature and also leads to α-hydroxyethyl radicals due to a 1,2-H shift[40] of the initially formed alkoxyethyl radical in reaction 10.

$$\bullet OH + C_2H_5OH \rightarrow H_2O + C_2H_5O\bullet \quad (9)$$

$$CH_3CH_2O\bullet \xrightarrow{H_2O} CH_3\bullet CHOH \quad (10)$$
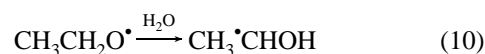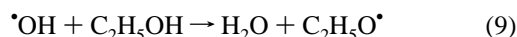
Reactions of H• and •OH with ethanol-d_6 (actually ethanol-d_5 when dissolved in light water) are similar to normal ethanol,

but abstraction of deuterium leads to a different gas product, as indicated in reaction 11.

$$H^{\bullet} + C_2D_5OH \rightarrow HD + (C_2D_4OH)^{\bullet}$$
$$k_{11} = 2.7 \times 10^6 \ (M^{-1} \ s^{-1})^{41} \quad (11)$$

$$^{\bullet}OH + C_2D_5OH \rightarrow HDO + (C_2D_4OH)^{\bullet}$$
$$k_{12} = 1.2 \times 10^9 \ (M^{-1} \ s^{-1})^{35,42} \quad (12)$$
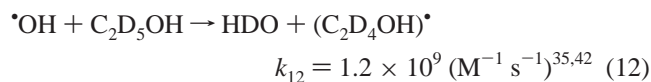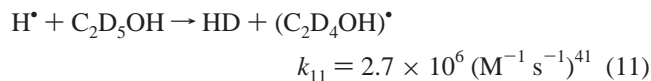
In this system, HD gives an easily detectable and specific ion mass signal corresponding to the hydrogen atom. The pairing of this deuterated alcohol in solution with N_2O then should allow simultaneous measurement of yields for molecular H_2, $H^{\bullet}$ atom (as HD), and hydrated electron (as N_2).

The temperature dependence of radiation yields of gaseous products determined in 0.02 *m* ethanol-d_6 solutions in the presence of N_2O is also plotted in Figure 5 to compare with the phenol results. Detailed values of the temperature dependence of radiation yields of gaseous products at 250 bar are included in Table 1. In comparing values of H_2 listed for both ethanol-d_6 and phenol, we see a very good agreement up to 300 °C. At temperatures of 350 °C and above we found higher yields of $H_2$ in ethanol-d_6. This was a surprise but was explained with the help of the competition experiment described below.

N_2 yields at room temperature and up to 100 °C for both ethanol-d_6 and phenol compare very well. This provides ex post facto validation of our dosimetry technique (see Experimental Section). However from 200 to 400 °C the yield of N_2 production in ethanol-d_6 solutions is higher than in phenol solutions (see Table 1). In N_2O aqueous solutions where formation of α-heteroradical is possible, additional production of nitrogen can occur. The α-hydroxyalkyl radicals formed in reactions 7, 8, 11, and 12 reduce nitrous oxide in reaction 13 to give nitrogen and hydroxyl radical. The product $^{\bullet}OH$ radical can then react with another ethanol-d_6 molecule via reaction 12 completing a free radical chain reduction of N_2O.

$$CD_3{}^{\bullet}CDOH + N_2O \rightarrow CD_3CDO + N_2 + {}^{\bullet}OH \quad (13)$$

Similar behavior was reported in the literature previously for methanol[43] and isopropanol[44] up to 310 °C. The chain reaction was also observed in our laboratory during high-temperature γ radiolysis of ethanol solutions, where due to substantially lower dose rate, reaction 13 was much more efficient, resulting in an order of magnitude higher N_2 yields than expected.[45] This problem forced us to ignore the N_2 yields from the ethanol experiments at high temperature and use phenol as the $H^{\bullet}$ and $^{\bullet}OH$ scavenger for the hydrated electron yield measurement.

The HD yield at room temperature is very low compared to earlier measurements of $H^{\bullet}$ atom yield, and we were not certain that a 0.02 *m* concentration of ethanol-d_6 gives enough scavenging power (5.4×10^4 s^{-1} at room temperature) to compete efficiently for $H^{\bullet}$ atoms with other second-order reactions or impurities. As a test we performed a series of experiments with 0.01 *m* (normal) ethanol aqueous solutions with 2.5×10^{-3} *m* N_2O. Figure S1 of the Supporting Information shows the radiation yields of H_2 in 0.01 *m* ethanol compared to the HD + H_2 yield in 0.02 *m* ethanol-d_6. Both yields compare well from 100 °C up to 300 °C, justifying the small concentration of ethanol-d_6 used for the $H^{\bullet}$ atom yield determination. The discrepancy at room temperature is obviously due to the 5 times lower scavenging power of ethanol-d_6. We could reproduce the same small yield with normal ethanol at 5 times lower concentration. At higher temperature the difference disappears
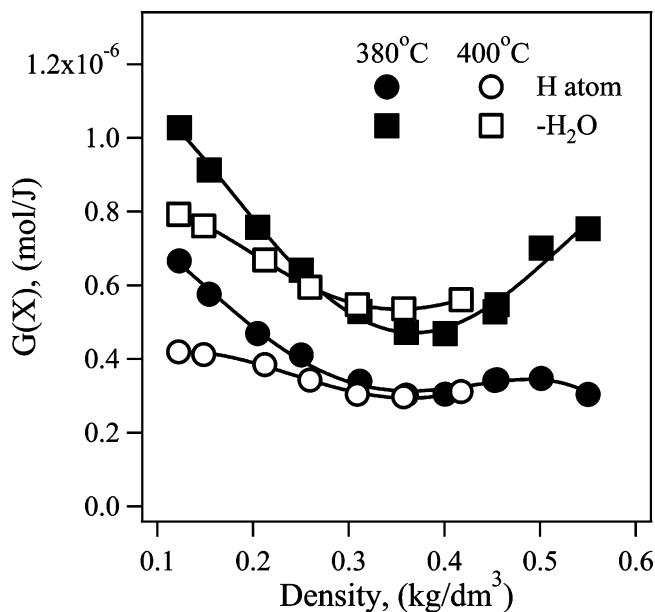
Figure 8. Water dissociation yield and corrected $H^{\bullet}$ atom yield vs density.
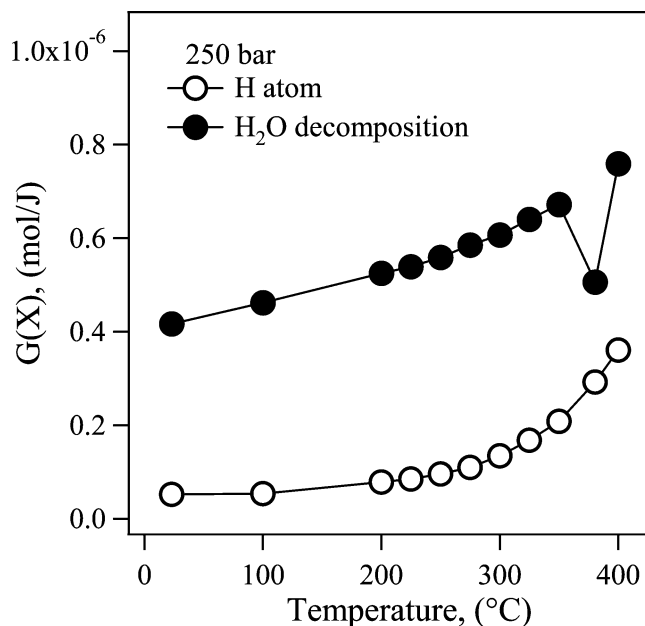
Figure 9. Water dissociation yield and corrected $H^{\bullet}$ atom yield vs temperature.

because the activation energy for reaction 11 is higher than that of reaction 7. For cost reasons we did not use a higher concentration of ethanol-d_6.

In light of all this information we measured the density dependence of radiation yields of gaseous products in 0.02 *m* ethanol-d_6 in supercritical water at 380 and 400 °C. In the range 0.12–0.54 kg/dm^3 at 380 °C, the density dependence of H_2 and HD yields demonstrates a U-like shape as seen before (Figure 6). Detailed results are listed in Table 2. At a temperature of 400 °C in the range 0.12–0.41 kg/dm^3 similar behavior is observed (Figure 7), but the HD yields are lower than at 380 °C. The detailed values are presented in Table 3. At both 380 and 400 °C the molecular H_2 yields in phenol solutions are significantly lower than for the corresponding ethanol-d_6 experiments. In the constant pressure experiments illustrated in Figure 5, a divergence of the H_2 yields for the two scavenging solutions can be seen starting above 325 °C.

Neutron and β/γ Radiolysis of Water

J. Phys. Chem. A, Vol. 111, No. 32, 2007 **7783**

The higher H_2 yields in ethanol-d_6 relative to phenol solutions at elevated temperature led us to ask what additional H_2 source could be present. Isotope exchange at the deuteroxyl group in C_2D_5OD in water is very fast already at room temperature, and therefore in all experiments the actual solute is C_2D_5OH. This alcohol hydroxyl group bears the only hydrogen available for abstraction by H-atoms that might contribute to the enhanced yield of H_2. As was mentioned above, the abstraction of hydrogen from the hydroxyl group is considerably less efficient than abstraction of hydrogen from any aliphatic carbon atom in an alcohol. Assuming higher activation energy for reaction 14 than for other competing D-abstractions in reaction 11, one can expect that with increase of temperature reaction 14 will play a more important role. In the Supporting Information we describe a competition experiment designed to show this is the correct explanation, and estimate the relative rates of reactions 14 and 11. Several other important cross-check experiments are also described.

$$H^{\bullet} + C_2D_5OH \rightarrow H_2 + C_2D_5O^{\bullet} \quad (14)$$
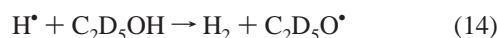
The behaviors of e_{aq}^-, $H^{\bullet}$ atom, and H_2 yields in the phenol and ethanol-d_6 scavenger systems are combined in Figures 6 and 7 for 380 and 400 °C. It can be seen that the apparent H_2 yield in the ethanol-d_6 system is nearly twice the yield in the phenol system. This is because of reaction 14 mentioned above. On the basis of the tests detailed in the Supporting Information, we believe the phenol system gives a correct estimate of the H_2 yield. To get correct $H^{\bullet}$ atom yields at high temperature, we should use the formula

$$G(H^{\bullet}) = G(HD, \text{ethanol-}d_6) + \\ G(H_2, \text{ethanol-}d_6) - G(H_2, \text{phenol}) \quad (15)$$

As noted in the Introduction, the object of modeling the chemistry is ultimately to determine the yield of production of H_2O_2 and H_2. H_2O_2 represents the combination of two oxidizing $^{\bullet}OH$ radicals. H_2 represents the combination of two reducing radicals (e_{aq}^- or $H^{\bullet}$). From the measurements shown above we are able to estimate a total yield of reducing equivalents, as

$$G(\text{red}) = G(e_{aq}^-) + G(H^{\bullet}) + 2G(H_2) \quad (16)$$

By mass balance, this must also equal the yield of oxidizing equivalents, and the yield of water dissociation:

$$G(\text{red}) = G(-H_2O) = G(\text{ox}) = G(^{\bullet}OH) + 2G(H_2O_2) \quad (17)$$

In Figure 8 we plot both the water dissociation yield and the corrected $H^{\bullet}$ atom yield as a function of density for 380 and 400 °C. In Figure 9 we plot both of these functions vs the temperature for 250 bar pressure. Two things become obvious from these plots. First, the total dissociation yield for water has increased a factor of over 2, in going from room temperature to low-density supercritical fluid. Second, the fraction of dissociation due to $H^{\bullet}$ atoms has increased dramatically in the low-density fluid.

IV. Discussion

In beginning a discussion of radiolysis G values, it is useful to clarify what is actually being measured. Low LET radiation dumps energy in relatively large chunks, which tend to be well separated spatially.[26,46] In γ radiolysis the dominant energy loss mechanism is Compton scattering. High-energy electrons (or
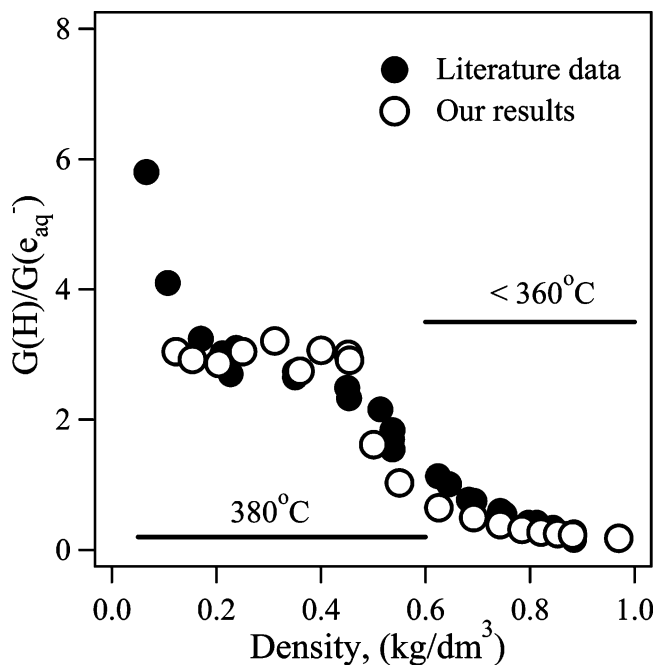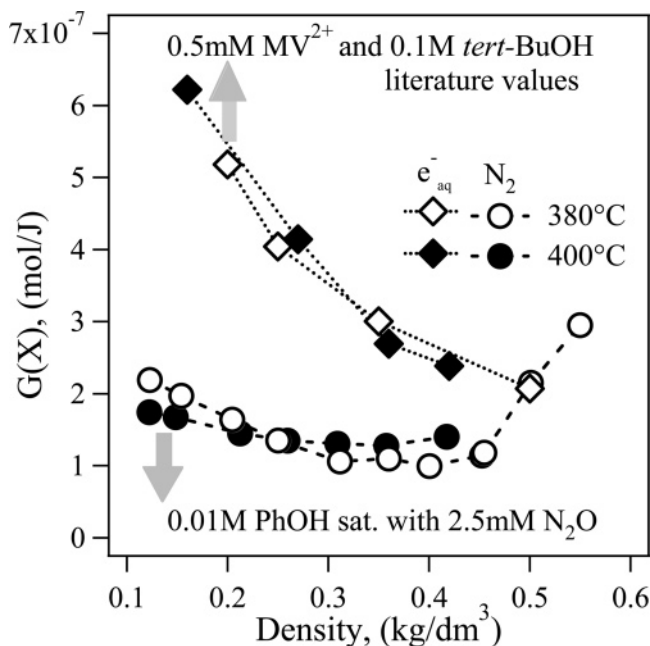

Figure 10. Comparison of the present ratio $G(H)/G(e_{aq}^-)$ with a direct measurement of the quantity from ref 10.

protons) act essentially as white light, exciting all dipole-allowed transitions via the coulomb perturbation.[30] In either case most primary excitations generate secondary electrons with energy in the $10-100$ eV energy range, which cause additional ionization and electronic excitations in close proximity to the primary event. The free radicals generated in these "spurs" will tend to recombine on timescales from picoseconds to microseconds; the G value (molecules/unit energy) for a given species is a function of time. For isolated spurs in three dimensions the radicals will diffuse apart to infinity, and it is meaningful to talk about an escape yield $G_{\infty}(X)$, but this is only an approximation in reality. Scavengers of one or more radical species act in competition with the recombination reactions; the higher the scavenging power (rate constant times concentration), the larger is the measured yield of product up to the limit of the "time zero" yield $G_0(X)$. Cooperative effects are also observed in which a scavenger for one species increases the escape yield of another.[47,48] In room-temperature water, escape yields are typically approximated with scavenging powers of 10^6 to 10^7 s^{-1}. Because the various scavenging reactions and recombination reactions have different activation energies, scavenger concentrations appropriate for room temperature might be unsuitable at high temperature. Thus, in comparing yields from different experiments at different temperatures, it is essential to take account of the scavenging rates and recombination rates of all species. Ultimately, a comprehensive stochastic model of the spur chemistry is required to correlate all of the data. This has been largely accomplished for room-temperature water,[26-29] but fundamental data are still being collected for elevated temperatures.

Keeping in mind differences in scavenging power as noted above, we find substantial agreement of the present results with earlier studies in subcritical water. Much of the earlier work was compiled and reviewed by Elliot and co-workers,[49,50] who summarized γ radiolysis G values as a set of linear functions of temperature. Our molecular H_2 yields are in agreement up to 300 °C. Inspection of the data used by Elliot and co-workers shows the electron and $H^{\bullet}$ atom yields were only measured up to 200 °C.[49,50] Up to 200 °C, we are in reasonable agreement.

Figure 11. Radiation yields for solvated electron in supercritical water. Comparison of the present study with the results of Lin et al.[17]

Our values for $G(N_2)$ in the phenol/N_2O system are 8% higher than Elliot's $G(e_{aq}^-)$, because of a higher scavenging power used. Our H$^\bullet$ atom (HD) yields from ethanol-d_6 are slightly lower than proposed by Elliot et al., mainly because of the low scavenging power of the ethanol-d_6 at lower temperature.

Between 200 and 300 °C our hydrated electron yields become essentially constant. This is in agreement with the finding of Sunaryu et al.[51] who carried out γ yield measurements up to 250 °C and found the same e_{aq}^- yield at both 200 °C and 250 °C. We also see substantial agreement with the pulse radiolysis study of Katsumura et al.,[19] who reported yields of $CO_3^{-\bullet}$ radical from both air- and N_2O-saturated 0.01 m carbonate solutions. The air-saturated solution gives signal from just the $^\bullet$OH radical yield and is a linear function of temperature, in agreement with Elliot et al.[49] The N_2O-saturated solutions represent the sum $G(^\bullet OH) + G(e_{aq}^-) + G(H^\bullet)$ because in the alkaline solution both reducing radicals are converted to $^\bullet$OH by the N_2O. The difference of the two sets of data gives a measure of $G(e_{aq}^-) + G(H^\bullet)$. There is a plateau region between 200 and 300 °C in agreement with our experiment. Above 300 °C the sum increases further, in qualitative agreement with the sharp rise in $G(H^\bullet)$ illustrated in Figure 9.

To our knowledge there are only two published sets of data that explore the radiolysis yields as a function of density in supercritical water. The first of these was the initial publication from Argonne,[10] which deduced the ratio $G(H^\bullet)/G(e_{aq}^-)$ as a function of density at 380 °C from the hydrated electron decay kinetics in 0.001 m KOH solution. In Figure 10 we superimpose the ratio $G(H^\bullet)/G(e_{aq}^-)$ from our product measurements on the ratio determined from kinetics. Good qualitative agreement is found throughout the density/temperature regime studied. (Quantitative agreement is not to be expected because the scavenging power for e_{aq}^- and H$^\bullet$ atoms was very different in the yield experiments, meaning that the two species are effectively measured at different times. In the kinetics experiments the "initial" ratio was deduced for a time on the order of 10 ns.)

The second study, which should be directly comparable, used methyl viologen transient absorption to measure yields in two experiments.[17] One experiment included 0.2 m ethanol to

scavenge $^\bullet$OH radicals and H$^\bullet$ atoms. The product α-hydroxy $CH_3{}^\bullet CHOH$ radical reduces methyl viologen as well, so the total radical yield $G(\text{radicals}) = G(e_{aq}^-) + G(^\bullet OH) + G(H^\bullet)$ can be estimated from the intense long-lived MV$^{+\bullet}$ cation radical absorbance at 605 nm. The result of this experiment is qualitatively in agreement with our results. In supercritical water at the lowest density, a total $G(\text{radicals})$ value of approximately 2.2×10^{-6} mol/J was reported at 400 °C. This number should be divided by 2 to estimate a lower limit for $G(-H_2O)$ of around 1.1×10^{-6} mol/J. The yield is slightly higher than our numbers for $G(-H_2O)$ in the same low-density limit, but this might be accounted for by the higher scavenging capacity being used (or an incorrect density, see below). A second experiment of this study included 0.2 m tertiary butanol to scavenge both $^\bullet$OH radical and H$^\bullet$ atoms. The scavenging was expected to produce a β-hydroxy radical that cannot reduce methyl viologen, and the absorbance should correspond to $G(e_{aq}^-)$ alone. The results of this experiment are plotted in Figure 11 along with our own measurements as a function of density at 380 and 400 °C. There is agreement at the highest density plotted, and also in subcritical water. (The plateau behavior between 200 and 300 °C is absent, but a large scavenging power of the doubly charged MV^{2+} might explain this.) But as the density decreases below 0.5 kg/dm^3 the methyl viologen-derived $G(e_{aq}^-)$ becomes much larger than our N_2 product yield, reaching a factor of 3 times larger at 0.15 kg/dm.^{3}

The methyl viologen experiments of ref 17 can be criticized in two respects. First, it is known that tertiary butanol dehydrates at high temperature,[52,53] and in the supercritical water cell the actual chemical system is probably methyl viologen with 0.2 m isobutene. H$^\bullet$ atoms and $^\bullet$OH radicals will add to isobutene at the double bond, producing carbon-centered "spectator" radicals as intended. (In fact, this should be a much better scavenger for H$^\bullet$ atoms than the tertiary butanol.) If the product radicals or the H$^\bullet$ atoms themselves were able to reduce MV^{2+}, it should occur on a longer time scale than e_{aq}^- scavenging and be visible in the kinetics, just as in the ethanol/MV^{2+} experiment. A far more important issue is that tertiary butanol or isobutene should have a very large partial molal volume due to its hydrophobic character.[54] The density of the supercritical fluid could be significantly lower than calculated for water alone. (We have noted such an effect with 0.1 m ethanol in supercritical water, where the observed H_2 signal decreased relative to lower ethanol concentration.) Whatever signal is observed is being divided by an assumed absorbed energy which is too large. This means the yields reported are almost certainly too small! Clearly recognition of this problem does not resolve the discrepancy in Figure 11.

The second issue is that the MV$^{+\bullet}$ extinction coefficient is not actually known at high temperature. Lin et al. demonstrate that the spectrum changes shape relatively little in supercritical water,[17] but the extinction coefficients used represent a guess based on the measurements below 200 °C. Still, it is hard to believe that this can possibly introduce an error of greater than 50%.

We have carefully considered whether our measurements of N_2 yield might be in error, and we find nothing that could explain the discrepancy with respect to Lin et al.[17] Moreover, we are in good agreement with the previous work at Argonne.[10] It is our conclusion that the $G(e_{aq}^-)$ numbers reported by Lin et al.[17] are much too large to represent the true e_{aq}^- escape yield in low-density supercritical water. On the other hand, as we noted above, our estimate of $G(-H_2O)$ is not in qualitative disagreement with Lin et al.'s evaluation of $G(\text{radicals})$, given

Neutron and β/γ Radiolysis of Water

J. Phys. Chem. A, Vol. 111, No. 32, 2007 **7785**

the difference in scavenging power and the probable density error from presence of 0.2 *m* ethanol. The most likely explanation is that some part of the H$^\bullet$ atom yield is not scavenged by the isobutene (or *t*-BuOH) and is able to reduce methyl viologen. This possibility was mentioned by Lin et al.[17] Quite probably a large part of the H$^\bullet$ atom yield comes from recombination of e_{aq}^- with protons in the spurs. This reaction might be intercepted by MV^{2+} scavenging of electrons, effectively converting H$^\bullet$ atom yield into MV$^{+\bullet}$ yield. It may also be that MV^{2+} acts as an exciton trap, scavenging water excitons that would otherwise dissociate water to H$^\bullet$ and $^\bullet$OH. The assumption involved here is that these excitons are somehow longer-lived in low-density supercritical water than in liquid water.

Setting aside this discrepancy for the time being, what do the yield measurements tell us about the radiolysis mechanism in high-temperature water? The $G(-H_2O)$ plotted in Figure 9 illustrates one major trend that has been deduced before.[10,17,49] At elevated temperature there is greater net dissociation of water, and correspondingly less spur recombination. Recent work[55] has confirmed and extended earlier measurements[56] to show that the rate of recombinations involving $^\bullet$OH radical are well below the diffusion limit above 100 °C. Moreover, the reaction of two hydrated electrons, which is diffusion limited below 150 °C, abruptly "turns off" at higher temperature.[57,58] Therefore diffusional escape of the radicals from spur recombination "wins" at elevated temperature. Another obvious effect is that at lower water densities the spurs will become "larger", further reducing the tendency for recombination. In low-density supercritical water the $G(-H_2O)$ reaches a value over twice that of room-temperature water. Similarly, the G(radicals) reported for 0.15 kg/dm^3 in ref 17 approach that for water vapor, suggesting relatively little recombination occurs.

A second trend illustrated in Figure 10 was already made obvious in the earlier work from Argonne.[10] H$^\bullet$ atoms are formed in lower density water rather than hydrated electrons. Two mechanisms can immediately be suggested. First, in water of lower dielectric constant the recombination of negatively charged e_{aq}^- with positively charged protons will be greatly enhanced, thus converting electrons into H$^\bullet$ atoms within the spurs. Second, cage escape of (H$^\bullet$, $^\bullet$OH) geminate pairs will be enhanced at elevated temperature and at lower densities, thus increasing both the overall radical yields and the relative yield of H$^\bullet$ atoms over electrons. A third less obvious mechanism has to do with the position of the water ionization threshold and the distribution of oscillator strength. In liquid water direct excitation of valence electrons into delocalized conduction band states can be accomplished with approximately 9.5 eV photons, whereas the water monomer ionization threshold is 12.6 eV.[59] Oscillator strength for the lowest electronic transitions of the vapor is shifted above the ionization continuum in liquid water.[60] Sukhonosov[61] has noted that this explains the ratio of ionization (e_{aq}^-) to electronic excitation (dissociation to H$^\bullet$, $^\bullet$OH) in liquid water. At low densities in supercritical water one expects the 9.5 eV threshold will shift back toward the 12.6 eV vapor-phase limit, and the oscillator strength will shift back toward the red. This will tend to favor neutral dissociation of water molecules (giving H$^\bullet$ and $^\bullet$OH) over ionization (giving e_{aq}^-, $^\bullet$OH, and H$^+_{aq}$).

It was also noted in earlier studies[49] that the rising $G(H_2)$ at higher temperature in subcritical water runs counter to the expectation of less radical recombination. (The hydrogen peroxide yield drops with temperature, as expected.[49]) It was suggested that the increase in $G(H_2)$ with temperature must come from a mechanism related to the early thermalization events in

spurs. More recently it has been shown that the "molecular" H$_2$ yield can be suppressed with good presolvated electron scavengers,[62] indicating that the H$_2$ comes from very fast recombination of electrons with H$_2$O$^+$, or else an electron capture resonance producing transient H$^-$ followed by its reaction with water giving H$_2$ and OH$^-$. Our observation of a substantial G value for molecular H$_2$ in the low-density supercritical fluid was a surprise, given the earlier remarks about the inefficiency of radical recombination. Apparently, one or both of the suggested mechanisms for molecular H$_2$ formation is favored at high temperature and low density. It seems very unlikely that prompt recombination of presolvated electrons with presolvated H$_2$O$^+$ is favored at low density (the spurs must be much larger, reducing the likelihood of the encounter), so we suggest the negative ion resonance giving transient H$^-$ as the probable mechanism for molecular H$_2$ formation under these conditions. We do not know why this mechanism would be enhanced at lower density and higher temperature. Perhaps the cross-section is strongly influenced by the number of hydrogen bonds formed by a given molecule. At low-density this average number of hydrogen bonds becomes much smaller than four.[63,64]

A most puzzling observation is the minimum in free radical yields $G(e_{aq}^-)$, $G(H^\bullet)$, and $G(-H_2O)$ in supercritical water of intermediate density (ca. 0.4 kg/dm^3). Surprisingly, a minimum in $G(H_2)$ is also found at the same density as the minimum in radical yields, suggesting that the minima are not related to radical recombination probabilities, but rather to early (photo)-physical events. Once again, we might suspect that the changing average local environment of water molecules (e.g., average number of hydrogen bonds) plays a large role in determining the chemical action spectrum of the low-energy secondary electrons. For example, recent ab initio calculations for water dimer to pentamer cluster excited states have demonstrated that the presence of an H-bond changes the lowest excited surface from unbound to bound for the O−H stretch.[65,66] Clearly, more data on the water deep (vacuum) UV spectrum is needed for these conditions, as well as more theoretical insight into the excited electronic processes.

Finally, what do the measured numbers mean for radiolytic production of hydrogen peroxide and hydrogen in a nuclear reactor? Given 5.2 eV to dissociate a water OH bond, the maximum possible G value for dissociation of water is on the order of 1.9 μmol/J. We see numbers in supercritical fluid at 380 °C on the order of 0.8−1.0 μmol/J. So the prompt efficiency of water dissociation approaches 50% of the absolute maximum under these conditions. What is the net G value for production of H$_2$ and H$_2$O$_2$ after all recombinations have run to completion? This depends mostly on the efficiency of the cross reaction H$^\bullet$ + $^\bullet$OH → H$_2$O relative to the homogeneous recombinations H$^\bullet$ + H$^\bullet$ → H$_2$ and $^\bullet$OH + $^\bullet$OH → H$_2$O$_2$ in bulk solution. H$^\bullet$ + H$^\bullet$ → H$_2$ is probably much faster than H$^\bullet$ + $^\bullet$OH → H$_2$O in supercritical water. This will favor the H$_2$ and H$_2$O$_2$ products over the recombination to re-form H$_2$O. Roughly speaking, the G value for H$_2$O$_2$ production should lie in the range $^1/_4$ to $^1/_2$ of the $G(-H_2O)$ that we have deduced here. Obviously this calculation pertains only to neat water chemistry and ignores any possible effects of impurities or additives.

V. Summary

G values for molecular H$_2$ and for the free radicals H$^\bullet$ and e_{aq}^- have been determined for electron radiolysis up to supercritical water temperature by a very precise mass spectroscopy technique using N$_2$O and ethanol-d_6 scavengers for e_{aq}^- and H$^\bullet$ atoms, respectively. Yields were also measured at

7786 *J. Phys. Chem. A, Vol. 111, No. 32, 2007*

Janik et al.

380 and 400 °C as a function of the water density. In agreement with earlier measurements, the yields of e_{aq}^- and H• both increase at elevated temperature, as does the yield of molecular H_2 and the total dissociation of water, $G(-H_2O)$. In supercritical water, the yield of H• atom becomes substantially larger than e_{aq}^-, especially at low density. Surprisingly, the yield of molecular H_2 does not tend toward zero, even though radical recombination must be much less probable at the lower densities. Also surprising is the observation of a minimum in all of the measured yields, both radical and molecular, in supercritical water at around 0.4 kg/dm.[3] We believe that both observations are related to changes in the aqueous electronic structure and photophysics as the average number of hydrogen bonds changes with density.

Supporting Information Available: A description of several cross-check experiments, with three figures and one table of auxiliary results. This material is available free of charge via the Internet at http://pubs.acs.org.

References and Notes

(1) Ma, B. M. *Nuclear Reactor Materials and Applications*; Van Nostrand Reinhold: New York 1983.
(2) Koshizuka, S.; Oka, Y. *Prog. Nucl. Energy* **1998**, *32*, 547.
(3) Oka, Y.; Koshizuka, S. *Prog. Nucl. Energy* **1998**, *32*, 163.
(4) Bushby, S. J.; Dimmick, G. R.; Duffey, R. B.; Burrill, K. A.; Chan, P. S. W. "Conceptual designs for advanced, high-temperature CANDU reactors"; ICONE 8: 8th International Conference on Nuclear Engineering, 2000, Baltimore, MD.
(5) Squarer, D.; Schulenberg, T.; Struwe, D.; Oka, Y.; Bittermann, D.; Aksan, N.; Maraczy, C.; Kyrki-Rajamaki, R.; Souyri, A.; Dumaz, P. *Nucl. Eng. Des.* **2003**, *221*, 167.
(6) Oka, Y.; Koshizuka, S. *J. Nucl. Sci. Technol.* **2001**, *38*, 1081.
(7) Takiguchi, H.; Ullberg, M.; Uchida, S. *J. Nucl. Sci. Technol.* **2004**, *41*, 601.
(8) Christensen, H. *Nucl. Technol.* **1995**, *109*, 373.
(9) McCracken, D. R.; Rasewych, J. B.; Shorter, W. R. "Coolant Radiolysis and Boiling in Water-Cooled Reactors"; Water Chemistry of Nuclear Reactor Systems 5, 1989, London.
(10) Cline, J.; Takahashi, K.; Marin, T. W.; Jonah, C. D.; Bartels, D. M. *J. Phys. Chem. A* **2002**, *106*, 12260.
(11) Marin, T. W.; Cline, J. A.; Takahashi, K.; Bartels, D. M.; Jonah, C. D. *J. Phys. Chem. A* **2002**, *106*, 12270.
(12) Takahashi, K.; Bartels, D. M.; Cline, J. A.; Jonah, C. D. *Chem. Phys. Lett.* **2002**, *357*, 358.
(13) Takahashi, K. J.; Ohgami, S.; Koyama, Y.; Sawamura, S.; Marin, T. W.; Bartels, D. M.; Jonah, C. D. *Chem. Phys. Lett.* **2004**, *383*, 445.
(14) Marin, T. W.; Jonah, C. D.; Bartels, D. M. *J. Phys. Chem. A* **2005**, *109*, 1843.
(15) Bartels, D. M.; Takahashi, K.; Cline, J. A.; Marin, T. W.; Jonah, C. D. *J. Phys. Chem. A* **2005**, *109*, 1299.
(16) Bonin, J.; Janik, I.; Janik, D.; Bartels, D. M. *J. Phys. Chem. A* **2007**, *111*, 1869.
(17) Lin, M. Z.; Katsumura, Y.; Muroya, Y.; He, H.; Wu, G. Z.; Han, Z. H.; Miyazaki, T.; Kudo, H. *J. Phys. Chem. A* **2004**, *108*, 8287.
(18) Wu, G. Z.; Katsumura, Y.; Lin, M. Z.; Morioka, T.; Muroya, Y. *Phys. Chem. Chem. Phys.* **2002**, *4*, 3980.
(19) Katsumura, Y.; Wu, G. Z.; Lin, M. Z.; Muroya, Y.; Morioka, T.; Terada, Y.; Li, X. F. *Res. Chem. Intermed.* **2001**, *27*, 755.
(20) Wu, G. Z.; Katsumura, Y.; Muroya, Y.; Lin, M. Z.; Morioka, T. *J. Phys. Chem. A* **2001**, *105*, 4933.

(21) Lin, M. Z.; Katsumura, Y.; He, H.; Muroya, Y.; Han, Z. H.; Miyazaki, T.; Kudo, H. *J. Phys. Chem. A* **2005**, *109*, 2847.
(22) Miyazaki, T.; Katsumura, Y.; Lin, M. Z.; Muroya, Y.; Kudo, H.; Asano, M.; Yoshida, M. *Radiat. Phys. Chem.* **2006**, *75*, 218.
(23) Miyazaki, T.; Katsumura, Y.; Lin, M. Z.; Muroya, Y.; Kudo, H.; Taguchi, M.; Asano, M.; Yoshida, M. *Radiat. Phys. Chem.* **2006**, *75*, 408.
(24) McCracken, D. R.; Tsang, K. T.; Laughton, P. J. "Aspects of the physics and chemistry of Water Radiolysis by Fast Neutrons and Fast Electrons in Nuclear Reactors," report AECL-11895, 1998.
(25) Laverne, J. A. *J. Phys. Chem.* **1988**, *92*, 2808.
(26) Pimblott, S. M.; LaVerne, J. A.; Mozumder, A. *J. Phys. Chem.* **1996**, *100*, 8595.
(27) Pimblott, S. M.; LaVerne, J. A. *J. Phys. Chem. A* **1997**, *101*, 5828.
(28) Pimblott, S. M.; LaVerne, J. A. *J. Phys. Chem. A* **2002**, *106*, 9420.
(29) LaVerne, J. A.; Stefanic, I.; Pimblottt, S. M. *J. Phys. Chem. A* **2005**, *109*, 9393.
(30) Spinks, J. W. T.; Woods, R. J. *An Introduction to Radiation Chemistry*, 3rd ed.; Wiley-Interscience: New York 1990.
(31) Buxton, G. V.; Greenstock, C. L.; Helman, W. P.; Ross, A. B. *J. Phys. Chem. Ref. Data* **1988**, *17*, 513.
(32) Czapski, G.; Peled, E. *Isr. J. Chem.* **1968**, *6*, 421.
(33) Janik, I.; Bartels, D. M.; Marin, T. W.; Jonah, C. D. *J. Phys. Chem. A* **2007**, *111*, 79.
(34) Buxton, G. V.; Mackenzie, S. R. *J. Chem. Soc., Faraday Trans.* **1992**, *88*, 2833.
(35) Anbar, M.; Meyerstein, D.; Neta, P. *J. Chem. Soc. B* **1966**, 742.
(36) Mvula, E.; Schuchmann, M. N.; von Sonntag, C. *J. Chem. Soc., Perkin Trans.* **2001**, *2*, 264.
(37) Park, H. R.; Getoff, N. *Z. Naturforsch., A: Phys. Sci.* **1992**, *47*, 985.
(38) Ervens, B.; Gligorovski, S.; Herrmann, H. *Phys. Chem. Chem. Phys.* **2003**, *5*, 1811.
(39) Asmus, K. D.; Mockel, H.; Henglein, A. *J. Phys. Chem.* **1973**, *77*, 1218.
(40) von Sonntag, C.; Schuchmann, H. P. *J. Photochem.* **1981**, *16*, 289.
(41) Mezyk, S. P.; Bartels, D. M. *J. Phys. Chem. A* **1997**, *101*, 1329.
(42) Bonifacic, M.; Armstrong, D. A.; Stefanic, I.; Asmus, K. D. *J. Phys. Chem. B* **2003**, *107*, 7268.
(43) Ryan, T. G.; Sambrook, T. E. M.; Freeman, G. R. *J. Phys. Chem.* **1978**, *82*, 26.
(44) Ryan, T. G.; Freeman, G. R. *J. Phys. Chem.* **1977**, *81*, 1455.
(45) Janik, D.; Janik, I.; Bartels, D. M. *Radiat. Phys. Chem.*, manuscript in preparation.
(46) Pimblott, S. M.; Laverne, J. A.; Mozumder, A.; Green, N. J. B. *J. Phys. Chem.* **1990**, *94*, 488.
(47) Laverne, J. A.; Pimblott, S. M. *J. Chem. Soc., Faraday Trans.* **1993**, *89*, 3527.
(48) Pimblott, S. M.; Laverne, J. A. *J. Phys. Chem.* **1992**, *96*, 8904.
(49) Elliot, A. J.; Chenier, M. P.; Ouellette, D. C. *J. Chem. Soc., Faraday Trans.* **1993**, *89*, 1193.
(50) Elliot, A. J. "Rate Constants and G-Values for the Simulation of the Radiolysis of Light Water Over the Range 0−300 °C," report AECL-11073, 1994.
(51) Sunaryo, G. R.; Katsumura, Y.; Hiroishi, D.; Ishigure, K. *Radiat. Phys. Chem.* **1995**, *45*, 131.
(52) Richter, T.; Vogel, H. *Chem. Eng. Technol.* **2003**, *26*, 688.
(53) Xu, X. D.; Antal, M. J.; Anderson, D. G. M. *Ind. Eng. Chem. Res.* **1997**, *36*, 23.
(54) Biggerstaff, D. R.; Wood, R. H. *J. Phys. Chem.* **1988**, *92*, 1988.
(55) Janik, I.; Bartels, D. M.; Jonah, C. D. *J. Phys. Chem. A* **2007**, *111*, 1835.
(56) Elliot, A. J.; McCracken, D. R.; Buxton, G. V.; Wood, N. D. *J. Chem. Soc., Faraday Trans.* **1990**, *86*, 1539.
(57) Christensen, H.; Sehested, K. *J. Phys. Chem.* **1986**, *90*, 186.
(58) Marin, T. W.; Takahashi, K.; Jonah, C. D.; Bartels, D. M. *J. Phys. Chem. A*, submitted for publication.
(59) Bartels, D. M.; Crowell, R. A. *J. Phys. Chem. A* **2000**, *104*, 3349.
(60) Onaka, R.; Takahashi, T. *J. Phys. Soc. Jpn.* **1968**, *24*, 548.
(61) Sukhonosov, V. Y. *High Energy Chem.* **1995**, *29*, 243.
(62) LaVerne, J. A.; Pimblott, S. M. *J. Phys. Chem. A* **2000**, *104*, 9820.
(63) Wernet, P.; Testemale, D.; Hazemann, J. L.; Argoud, R.; Glatzel, P.; Pettersson, L. G. M.; Nilsson, A.; Bergmann, U. *J. Chem. Phys.* **2005**, *123*, 154503.
(64) Skarmoutsos, I.; Samios, J. *J. Phys. Chem. B* **2006**, *110*, 21931.
(65) Chipman, D. M. *J. Chem. Phys.* **2005**, *122*.
(66) Chipman, D. M. *J. Chem. Phys.* **2006**, *124*, 044305.